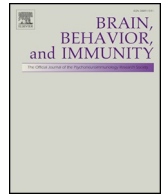# Mechanical pain of the lower extremity after compression of the upper spinal cord involves signal transducer and activator of transcription 3-dependent reactive astrocytes and interleukin-6

大野，瑛明

KYUSHU UNIVERSITY

Mechanical pain of the lower extremity after compression of the upper spinal cord involves signal transducer and activator of transcription 3-dependent reactive astrocytes and interleukin-6

Teruaki Ono[a,b], Yuta Kohro[a], Keita Kohno[a], Hidetoshi Tozaki-Saitoh[a], Yasuharu Nakashima[b], Makoto Tsuda[a,*]

[a] *Department of Life Innovation, Graduate School of Pharmaceutical Sciences, Kyushu University, 3-1-1 Maidashi, Higashi-ku, Fukuoka 812-8582, Japan*
[b] *Department of Orthopedic Surgery, Graduate School of Medical Sciences, Kyushu University, 3-1-1 Maidashi, Higashi-ku, Fukuoka 812-8582, Japan*

ABSTRACT

Chronic pain is one of the main symptoms of spinal disorders such as spinal canal stenosis. A major cause of this pain is related to compression of the spinal cord, and chronic pain can develop at the level of the compressed spinal segment. However, in many patients chronic pain arises in an area that does not correspond to the compressed segment, and the underlying mechanism involved remains unknown. This was investigated in the present study using a mouse model of spinal cord compression in which mechanical pain of the hindpaws develops after compression of the first lumbar segment (L1) of the spinal cord. Compression induced the activation of astrocytes in the L1 spinal dorsal horn (SDH)—but not the L4 SDH that corresponds to the hindpaws—and activated signal transducer and activator of transcription 3 (STAT3). Suppressing reactive astrocytes by expressing a dominant negative form of STAT3 (dnSTAT3) in the compressed SDH prevented mechanical pain. Expression of interleukin (IL)-6 was also upregulated in the compressed SDH, and it was inhibited by astrocytic expression of dnSTAT3. Intrathecal administration of a neutralizing anti-IL-6 antibody reversed the compression-induced mechanical pain. These results suggest that astrocytic STAT3 and IL-6 in the compressed SDH are involved in remote mechanical pain observed in the lower extremity, and may provide a target for treating chronic pain associated with spinal cord compression such as spinal canal stenosis.

1. Introduction

Nociceptive information from the periphery is processed in the spinal dorsal horn (SDH). The accurate perception of pain requires properly wired neuronal circuits and their correct functioning in the SDH. After spinal cord injury or compression however, nociceptive signaling can be pathologically and persistently altered. Chronic pain is a well-known symptom of spinal disorders such as spinal canal stenosis, in which the spinal cord is compressed by hypertrophied ligamentum flavum. Previous studies suggest that in many patients chronic pain can arise in an area that does not correspond to the compressed segment such as a lower extremity, in addition to chronic pain at the level of the compressed spinal segment (Chan et al., 2011; Ito et al., 1999). Given that the gold standard therapy for spinal cord compression-induced pain is surgical removal or correction of the source of compression, it is conceivable that such chronic pain of a lower extremity involves a remote signal or stimulus from the compressed spinal cord. Notably however, the underlying mechanisms involved remain unclear.

In the current study, compression of the spinal cord at the L1 segment was used to induce mechanical pain in the hindpaws of mice—an anatomical location that is mainly associated with the L4 segment—and the potential involvement of reactive astrocytes, signal transducer and activator of transcription 3 (STAT3), and interleukin (IL)-6 in the relevant mechanisms was investigated.
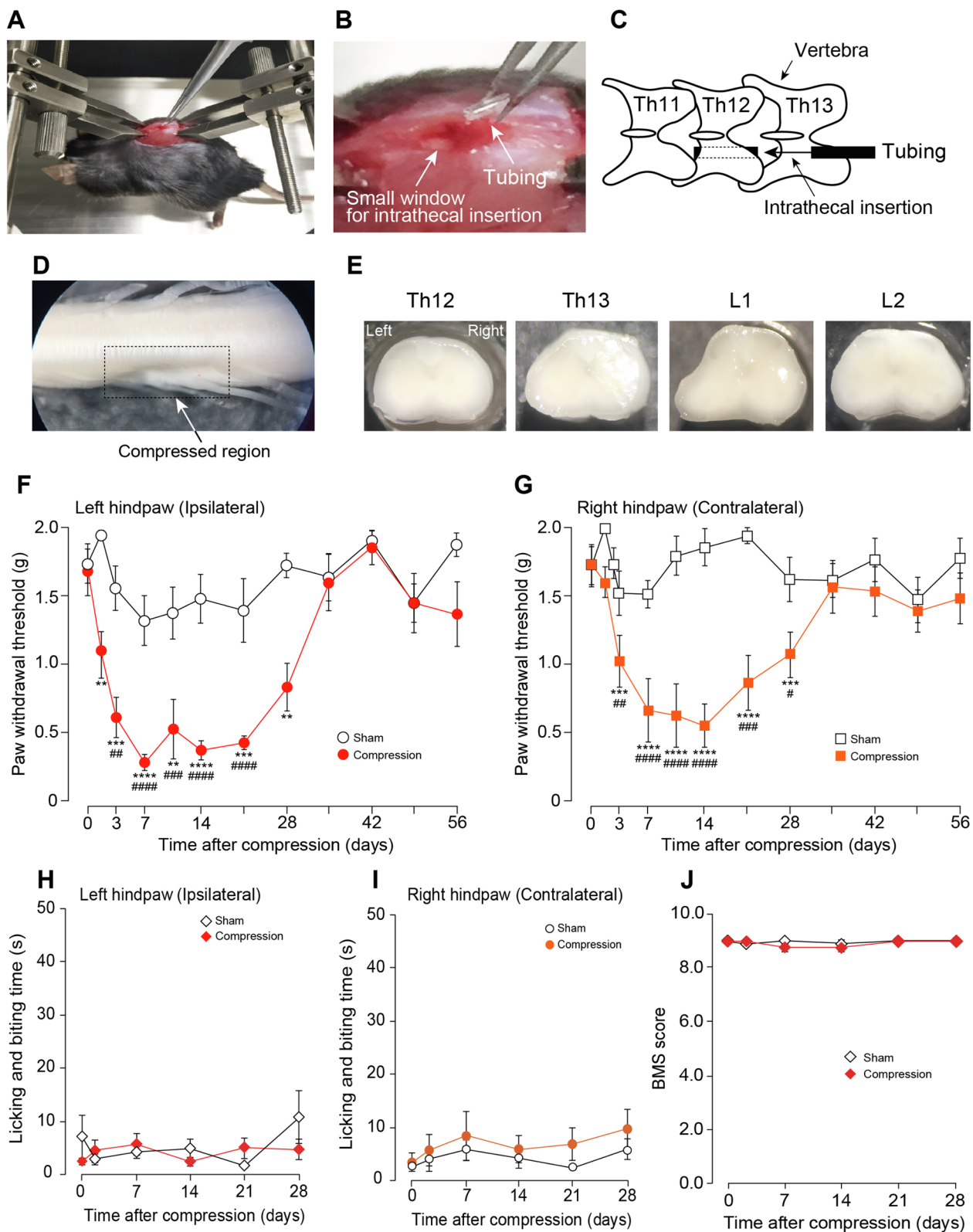
Fig. 1. Remote mechanical hindpaw pain in mice caused by compression of L1 in the spinal cord. (A) Photograph depicting the insertion of flexible tubing into the intrathecal space via forceps in a mouse restrained by attaching custom-made clamps to the vertebral column. (B) High–magnification view of the insertion. (C) Schematic illustration of insertion of the tubing into the intrathecal space under the Th12 vertebra. (D) Photograph of the compressed spinal cord. The rectangular area outlined with a dotted black line is the compressed region. (E) Photographs of spinal cord slices at Th12, Th13, L1, and L2 segments. (F, G) PWT in the left (ipsilateral; F) and right (contralateral; G) hindpaws of mice after spinal cord compression ($n = 8$) and after the sham operation ($n = 10$). **$P < 0.01$, ***$P < 0.001$ and ****$P < 0.0001$ versus the sham-operated group, two-way ANOVA with post hoc Bonferroni test. #$P < 0.05$, ##$P < 0.01$, ###$P < 0.001$, and ####$P < 0.0001$ versus the value at 0, one-way ANOVA with Tukey's multiple comparison test. Data show mean ± SEM. (H, I) Time spend in licking and biting behaviors to the left (ipsilateral; H) and right (contralateral; I) hindpaws before and after spinal cord compression ($n = 6$). (J) Basso Mouse Scale (BMS) Score of the hindlimbs after spinal cord compression or sham-operation ($n = 6$). Data show mean ± SEM.

2. Methods

2.1. Animals

Male C57BL/6J mice (CLEA Japan, Tokyo, Japan) were used. All mice used were 8–12 weeks of age at the start of each experiment, were housed at 22 ± 1 °C with a 12-h light–dark cycle and were fed food and water ad libitum. All animal experiments were conducted according to relevant national and international guidelines contained in the 'Act on Welfare and Management of Animals' (Ministry of Environment of Japan) and 'Regulation of Laboratory Animals' (Kyushu University) and under the protocols approved by the Institutional Animal Care and Use committee review panels at Kyushu University.

2.2. Spinal cord compression

Mice were deeply anesthetized by s.c. injection of ketamine (100 mg/kg) and xylazine (10 mg/kg). The skin was incised at the Th11–L2 vertebrae, and custom-made clamps were attached to the rostral and caudal sites of the vertebral column (Fig. 1A). Paraspinal muscles around the left side of the interspace between Th12 and Th13 vertebrae were removed. The space between the spinal cord and the vertebrae was gently enlarged using forceps. Flexible fluorine resin tubing with an outer diameter of 0.6 mm and an inner diameter of 0.4 mm (As One Corporation, Osaka, Japan) was cut to the size of one murine vertebra (an approximate length of 1.5 mm) and inserted into the intrathecal space (Fig. 1B, C). During this process care was taken not to puncture the spinal cord. After insertion, the skin was sutured with 3–0 silk, and the mice were monitored on a heating pad until they had recovered. If paralysis of the hindlimbs was observed immediately after spinal cord compression, the mice were excluded from the study. In the sham operations the paraspinal muscles were removed and the spinal cord was exposed.

2.3. Immunohistochemistry

Mice were deeply anesthetized by i.p. injection of pentobarbital (100 mg/kg) and transcardially perfused with phosphate-buffered saline (PBS), followed by ice-cold 4% paraformaldehyde (PFA)/PBS. The transverse L1 and L4 segments of the spinal cord were removed, post-fixed in the same fixative for 3 h at 4 °C, and placed in 30% sucrose solution for 24 h at 4 °C. Sections of the transverse L1 and L4 spinal cord (30 μm) were immunostained according to our previous method (Kohro et al., 2015). Primary and secondary antibodies used were listed below. Primary antibodies: monoclonal rat anti-glial fibrillary acidic protein (GFAP; 1:1000, Invitrogen, 13–0300, CA, USA), polyclonal rabbit anti-STAT3 (1:1000, Cell signaling, 9132S, MA, USA), polyclonal rabbit anti-ionized calcium-binding adapter molecule (IBA1; 1:5000, Wako, 019–19741, Osaka, Japan), monoclonal mouse anti-neuronal nuclei (NeuN; 1:2000, Abcam, ab104224, MA, USA), polyclonal goat anti-SRY-box transcription factor 9 (SOX9; 1:1000, R&D Systems, AF3075, MN, USA), monoclonal mouse anti-adenomatous polyposis coli (APC; CC1 clone, 1:500, Calbiochem, CA, USA), monoclonal rat anti-CD11b antibody (OX-42; 1:2000, Bio Rad, 707, California, USA) and polyclonal rabbit anti-GFP (1:2000, MBL, 077, Nagoya, Japan) and. Following incubation, tissue sections were washed and incubated for 3 h at room temperature in secondary antibody solution (Alexa Fluor 488 and/or 546, 1:1000, Molecular Probes, OR, USA). The tissue sections were washed, slide-mounted and subsequently cover-slipped with Vecta-shield hardmount with or without 4′,6-diamidino-2-phenylindole (DAPI) (Vector Laboratories, PA, USA). Three to five sections from the L1 and L4 spinal cord of each mouse were randomly selected and analyzed using an LSM 700 Imaging System (Carl Zeiss, Oberkochen, Germany). For the quantification of GFAP levels, the intensity of GFAP immunofluorescence (in the square (100 × 100 μm)) in the superficial and deep regions of the compressed L1 SDH was measured using the LSM 700 Imaging System.

For c-FOS immunostaining in the SDH, the plantar surface of the hindpaw of mice on day 3 after compression was stimulated for 5 min without anesthesia with a von Frey filament (0.6 g; interval, 1 sec). At 1.5 h after the mechanical stimulation, mice were deeply anesthetized by isoflurane and fixed by PFA as describe above. Transverse L4 spinal cord (30 μm) section was immunostained by primary antibodies: rabbit monoclonal anti-c-FOS (Cell signaling, 2250, 1:7500; MA, USA), monoclonal mouse anti-NeuN (1:2000, Abcam, ab104224, MA, USA) and isolectin B4 (IB4, a marker of non-peptidergic C fibres whose central terminals are located seletively in lamina IIi; 1:1000, Thermo Fisher, I21414, USA). For quantification, four sections from the L4 spinal cord segments were randomly selected from each mouse, and the number of c-FOS-positive neurons in the superficial lamina I–IIo was counted with ImageJ (http://rsbweb.nih.gov/ij/) as described previously (Koga et al., 2017).

2.4. Behavioral studies

To assess mechanical pain, mice were placed individually in an opaque plastic cylinder, which was placed on a wire mesh and habituated for 0.5–1 h to allow acclimatization to the new environment. After that, calibrated von Frey filaments (0.02–2.0 g, North Coast Medical, CA, USA) were applied to the plantar surfaces of the hindpaws of mice with or without spinal cord compression from below the mesh floor, and the 50% paw withdrawal threshold was determined using the up-down method (Chaplan et al., 1994). von Frey test was carried out at 0 (pre), 1, 3, 7, 10, 14, 21, 28, 35, 42, 49 and 56 days after spinal cord compression. In experiments examining the effect of an interleukin (IL)-6- or IL-1β-neutralizing antibody, von Frey test was carried out before (Pre) and 3 days after spinal cord compression (0), and 30, 60, 90, 120, 150 and 180 min, and 24, 48 and 72 hr after the intrathecal injection of each antibody. Locomotor function of the hindlimbs was assessed using Basso Mouse Scale (BMS) up to 28 days post-spinal cord compression by two-independent observers. Briefly, mice were placed in an open field (diameter: 1 m) and observed for 4 min. The score was made by a scale of 0–9 which was based on hindlimb movements made in an open field (Basso et al., 2006).

2.5. Vector construction and rAAV production

According to our previous study (Kohro et al., 2015), to produce recombinant adeno-associated virus (rAAV) vector for astrocyte-specific gene transduction, a vector containing the astrocytic promoter gfaABC$_1$D (Lee et al., 2008) was generated from pZac2.1 by substituting the CMV promoter with gfaABC$_1$D (amplified from addgene #19974). We then cloned AcGFP (referred to as GFP), the dominant-negative form of STAT3 (dnSTAT3; amplified from addgene #8709) and the constitutively active form of STAT3 (caSTAT3, amplified from addgene #13373) into the above modified pZac2.1 to generate pZac2.1-gfaABC$_1$D-GFP, pZac2.1-gfaABC$_1$D-dnSTAT3 and pZac2.1-gfaABC$_1$D-caSTAT3, respectively. The rAAV vector was produced from human embryonic kidney 293 (HEK293) cells with triple transfection [pZac, cis plasmid; pAAV2/5, trans plasmid; pAd DeltaF6, adenoviral helper plasmid (all plasmids were purchased from the University of Pennsylvania Gene Therapy Program Vector Core)] (Lock et al., 2010; Vandenberghe et al., 2010) and purified by two cesium chloride density gradient purification steps (Ayuso et al., 2010). The vector was dialyzed against PBS containing 0.001% (v/v) Pluronic-F68 using Amicon Ultra 100 K filter units (Millipore, Darmstadt, Germany). The Genome titre of rAAV was determined by Pico Green fluorometric reagent (Molecular Probes, OR, USA) following denaturation of the AAV particle. Vectors were stored in aliquots at −80 °C until use.

2.6. Intra-SDH injection of rAAV vector

We used the intra-SDH microinjection method with some modifications (Kohro et al., 2015). The skin was incised at Th11–L2, and custom-made clamps were attached to the rostral and caudal sites of the vertebral column. The paraspinal muscles around the left side of the interspaces of Th12/Th13 vertebrae were removed, and the dura mater and the arachnoid membrane were carefully incised using the tip of a 30G needle to make a small window to allow the microcapillary Femtotip (Eppendorf, NY, USA) insert directly into the SDH. The place where microcapillary inserted was under the Th12 vertebra. The microcapillary was inserted into the SDH (200–300 μm in depth from the surface of the dorsal root entry zone) through the small window. rAAV solutions (approximately 500–600 nl) were pressure-ejected using the FemtoJet Express (Eppendorf, NY, USA). After microinjection, the inserted microcapillary was removed from the SDH, the skin was sutured with 3–0 silk, and mice were kept on a heating pad until recovery. We used virus-injected mice for further analysis 28 days after injection. The viral titers of viruses were 1.0×10^{12} GC/ml determined by previous method (Kohro et al., 2015).

2.7. Quantitative real-time PCR

Mice were deeply anesthetized with pentobarbital (100 mg/kg, i.p.), perfused transcardially with PBS, the L1 and L4 spinal cord were removed and separated half at middle of the spinal cord by a sagittal cut. Samples contained the spinal cord ipsilateral or contralateral to the compression. Total RNA from the L1 and L4 spinal cord was extracted using Trisure (Bioline, London, UK) according to the manufacturer's protocol and our previous study (Kohro et al., 2015), and purified with RNeasy mini plus kit (Qiagen, CA, USA). The amount of total RNA was quantified by measuring the OD_{260} using a Nanodrop spectrophotometer (Nanodrop, DE, USA). For reverse transcription, 200 ng of total RNA was transferred to the reaction with Prime Script reverse transcriptase (Takara, Kyoto, Japan). Quantitative polymerase chain reaction (PCR) was carried out with Fast Start Essential DNA Probe Master (Roche, BSL, Switz) using a LightCycler 96 system (Roche, BSL, Switz). Expression levels were normalized with the average of the levels of *Gapdh* (glyceraldehyde-3-phosphate dehydrogenase) and *Actb* (β-actin) mRNAs. The sequence of TaqMan probe and forward and reverse primers used in this study were described as follows: *Aif1* (IBA1): 5′-FAM-CAGGAAGAGAGGCTGGAGGGGATCAA-TAMRA-3′ (probe), 5′-GATTTGCAGGGAGGAAAAGCT-3′ (forward primer), 5′-AACCCCAA GTTTCTCCAGCAT-3′ (reverse primer). *Tnfa* (tumor necrosis factor α (TNFα)): 5′-FAM-TACGTGCTCCTCACCCACACCGTCA-TAMRA-3′ (probe), 5′-GTTCTCTTCAAGGGACAAGGCTG-3′ (forward primer), 5′-TCCTGGTATGAGATAGCAAATCGG-3′ (reverse primer). *Il1b*: 5′-FAM-TGCAGCTGGAGAGTGTGGATCCCAA-TAMRA-3′ (probe), 5′ GAAAGACGGCACACCCACC-3′ (forward primer), 5′-AGACAAACCGCT TTTCCATCTTC-3′ (reverse primer). *Il6*: 5′-FAM-TCACAGAGGATACCA CTCCCAACAGACCTG-TAMRA-3′ (probe), 5′-GGGACTGATGCTGGTGA CAA-3′ (forward primer), 5′-TGCCATTGCACAACTCTTTTCT-3′ (reverse primer). *Gapdh*: 5′-FAM-ACCACCAACTGCTTAGCCCCCCTG-TAMRA-3′ (probe), 5′-TGCCCCCATGTTTGTGATG-3′ (forward primer), 5′-GGCAT GGACTGTGGTCATGA-3′ (reverse primer). *Actb*: 5′-FAM-CCTGGCCTC ACTGTCCACCTTCCA-TAMRA-3′ (probe),

5′-CCTGAGCGCAAGTACTCTGTGT-3′ (forward primer), 5′-CTGCTT GCTGATCCACATCTG-3′ (reverse primer). The primers and probe for *Itgam* (integrin αM) were obtained from Integrated DNA Technologies (IA, USA).

2.8. Drug administration

For intrathecal injections, a 30 G needle attached to a Hamilton micro-syringe was inserted between the L5/L6 vertebrae and then punctured through the dura (Hylden and Wilcox, 1980). The following drugs and dose were used for intrathecal injection experiments: mouse IL-6-neutralizing antibody (10 ng; MAB406-100, R&D Systems, Minneapolis, MN, USA; dissolved in saline), mouse IL-1β-neutralizing antibody (5 μg; AF-401-NA, R&D Systems, Minneapolis, MN, USA; dissolved in saline) and normal goat IgG control (10 ng and 5 μg; AB-108-C, R&D Systems, Minneapolis, MN, USA; dissolved in saline) (Kawasaki et al., 2008a; Morioka et al., 2018).

2.9. Flow cytometry

Mice were deeply anesthetized by i.p. injection of pentobarbital and perfused transcardially with PBS to remove circulating blood from the vasculature. The L1 and L4 spinal cord were rapidly and carefully removed. After meninges and dorsal roots were completely removed, spinal cords were separated half at middle of the spinal cord by a sagittal cut. Samples contained the spinal cord ipsilateral or contralateral to the compression. According to our previous study (Tashima et al., 2016), spinal tissue pieces were treated with pre-warmed enzymatic solution [0.2 U/mL Collagenase D (Roche, 11088866001, Mannheim, Germany) and 4.3 U/mL of Dispase (GIBCO, 17105041, NY, USA)] in Hanks' Balanced Salt Solution (HBSS) (+) containing 2% FBS for 30 min at 37 ˚C. The tissues were homogenized by passing through a 23G needle attached with a 1-mL syringe and were further incubated for 15 min at 37 ˚C. After that, the tissues were homogenized by passing twice through a 26G needle, and the enzymatic reaction was stopped by adding EDTA (20 mM). After washing to remove enzyme solution, the cell suspension was blocked by incubating with Fc Block (BD Pharmingen, 553142, San Diego, USA, 5 min, 4 ˚C) and immunostained with CD11b-Alexa Fluor 647 (1:1000, BD Pharmingen, 557686, San Diego, USA), CD45-APC-Cy7 (1:1000, Biolegend, 557659, San Diego, USA), Ly6C-PerCP Cy5.5 (1:400, BD Pharmingen, 560525, San Diego, USA) and CD4-PE (1:400, BD Pharmingen, 557308, San Diego, USA) for 30 min at 4 ˚C in the dark. After washing, the pellet was resuspended in ice-cold HBSS(-) containing 2% FBS and filtered through a 35-μm nylon cell strainer (BD Biosciences, San Jose, USA) to isolate tissue debris from the cell suspension. The total number of microglia ($CD11b^+$ $CD45^{int}$), monocytes/macrophages ($CD11b^+$ $CD45^{high}$ $Ly6C^+$), and $CD4^+$ T-cells ($CD11b^{neg}$ $CD45^{high}$ $CD4^+$) in the L1 and L4 spinal cord was analyzed using a flow cytometer (FACSVerse; BD Bioscience) and FlowJo software (TreeStar).

2.10. Statistical analysis

All data are shown as the mean ± SEM. Statistical significance of differences was determined using two-way ANOVA with post hoc Bonferroni test, one-way ANOVA with post hoc Dunnett's comparison test or Tukey's multiple comparison test using GraphPad Prism 8 software. Differences were considered significant at $P < 0.05$.

3. Results

3.1. Spinal cord compression-induced remote mechanical pain

To investigate chronic pain of the lower extremity after compression of the upper spinal cord, mice with L1 spinal cord compression (Fig. 1D, E; also see Methods) were used to test mechanical pain behaviors by measuring paw withdrawal thresholds (PWT) in response to mechanical stimulation. In sham-operated mice there was no significant reduction in PWT on the left or right sides (Fig. 1F, G), but spinal cord compressed mice became hypersensitive to the mechanical stimuli. PWTs on the left (ipsilateral) side were markedly reduced from day 1 (Fig. 1F), and these reductions peaked at day 7. The hypersensitivity persisted for at least 3 weeks, then the mice gradually recovered. Immunohistochemistry using the neuronal activity marker c-FOS confirmed that the number of c-FOS-positive neurons in the L4 SDH after mechanical stimulation was significantly increased in spinal cord compressed mice (Sup. 1).
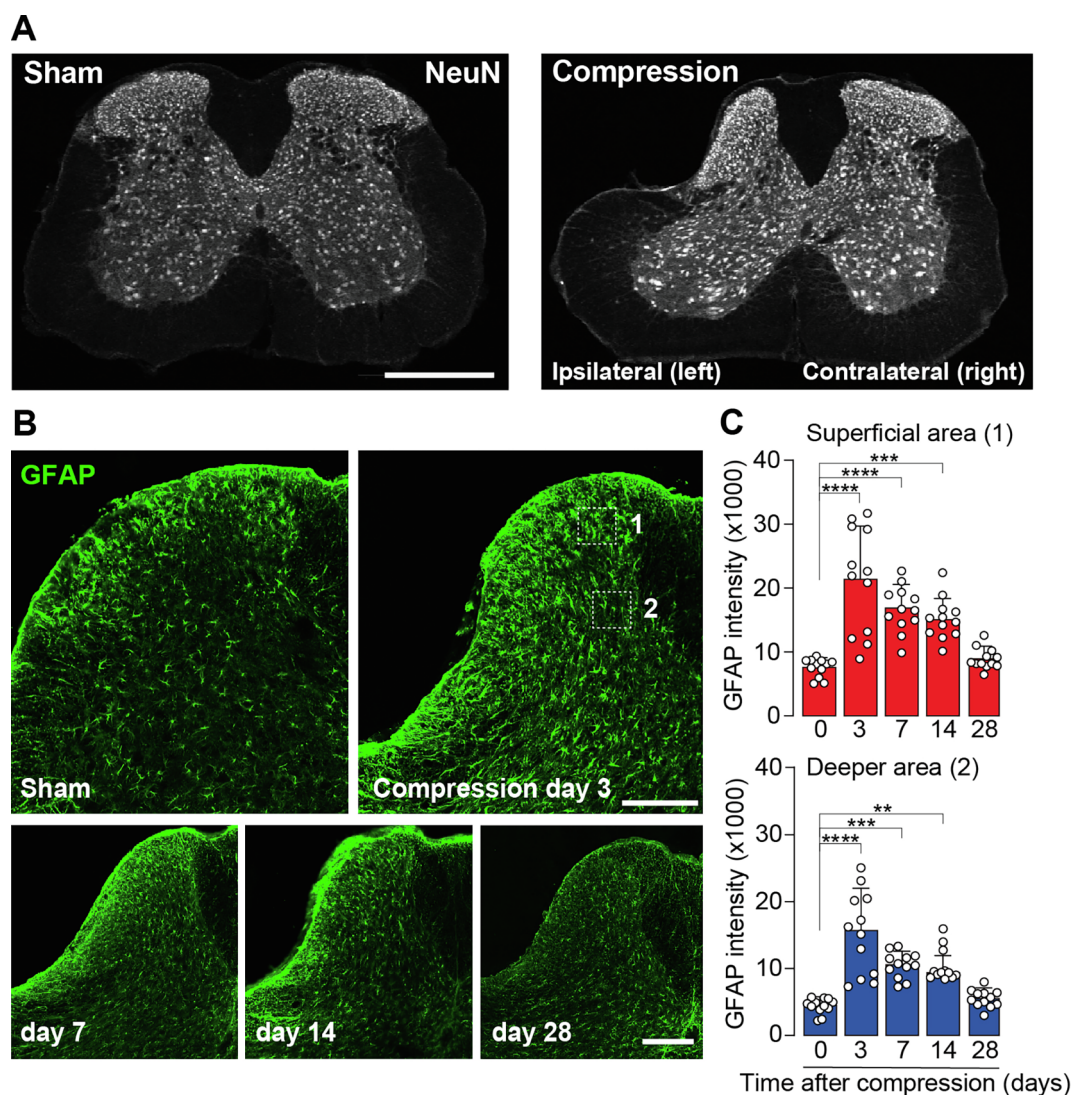
Fig. 2. Activation of astrocytes in the compressed spinal cord. (A) NeuN immunofluorescence in the compressed spinal cord (L1 segment) of mice 28 days after the compression or sham-operation. (B) Temporal pattern of GFAP immunofluorescence in the compressed SDH. (C) Quantitative analyses of GFAP immuno-fluorescence intensity at the L1 segment of mice before (day 0) and after spinal cord compression. Values represent the intensity to each timepoint (days 0 (naïve), 3, 7, 14, and 28). **$P < 0.01$, ***$P < 0.001$, and ****$P < 0.0001$, one-way ANOVA with Tukey's multiple comparison test. Data show mean ± SEM. Scale bars, 500 µm (A), 200 µm (B).

Interestingly, reductions in PWT were also observed in the right hindpaw (Fig. 1G). In this model, spontaneous licking and biting behaviors were not observed (Fig. 1H, I). In addition, neither a locomotor deficit (Fig. 1J) nor a cavity in the spinal cord (Fig. 2A) were also observed. Thus, these results suggest that spinal cord compression induces bilateral mechanical pain without impairing motor behavior.

3.2. Remote pain involves reactive astrocytes in the compressed SDH

Based on the above-described results indicating the induction of mechanical pain in bilateral hindpaws after compression of the upper spinal cord, it was surmised that the remote mechanical pain may be associated with an inflammatory signal generated at the compressed region. To investigate this, the potential involvement of astrocytes—which are abundant glial cells in the central nervous system (CNS) with a capacity to modulate pain signaling in the SDH (Ji et al., 2019)—was explored. Compared with sham-operated mice, there was a marked increase in immunofluorescent staining for the astrocyte marker GFAP in compressed SDHs (Fig. 2B). Levels of SDH GFAP immunoreactivity were significantly increased from day 3 to day 14 after compression,

and by day 28 GFAP immunoreactivity was weak (Fig. 2B, C). On the contralateral side of the compression, there was no remarkable increase in GFAP immunoreactivity compared with the sham-operated group from days 3–28 (Sup. 2). GFAP levels were not increased in the L4 segment of the SDH (Sup. 3). These results suggested that astrocytes were activated in the compressed L1 SDH, but not in the intact L4 SDH which corresponds to the hindpaws. In addition, spinal cord compression also increased the number of CD11b⁺ CD45^high Ly6C⁺ monocytes/macrophages and CD4⁺ T-cells (and resident microglia (CD11b⁺ CD45^int) as well) in the ipsilateral side of the L1 spinal cord (Sup. 4), suggesting infiltration of peripheral immune cells and activation of resident microglia in the compressed region.

To further investigate the role of reactive astrocytes in spinal cord compression-induced remote pain, the potential involvement of STAT3 was explored. STAT3 is a crucial transcription factor associated with astrocytic activation in a variety of models of CNS diseases including spinal cord injury (Herrmann et al., 2008; Okada et al., 2006), and there is evidence that astrocytic STAT3 in the SDH contributes to neuropathic pain (Kohro et al., 2015; Tsuda et al., 2011). In the current study there was an increase in STAT3 immunoreactivity in the L1
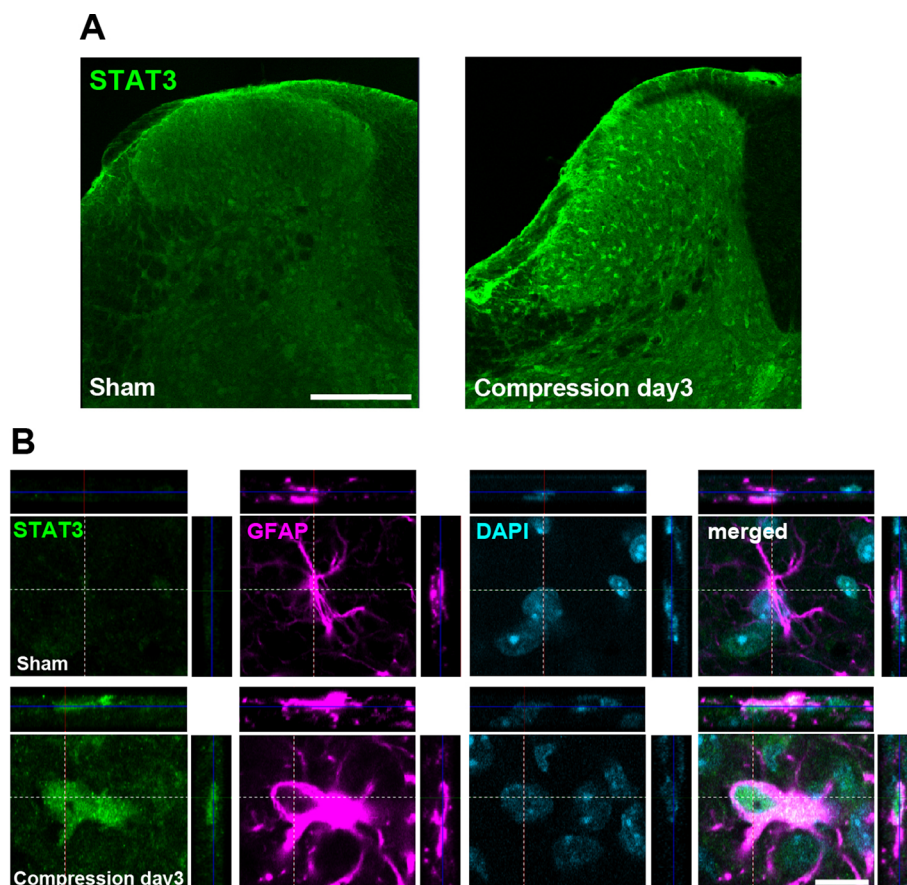
A

B

segment 3 days after compression, compared to sham-operated mice (Fig. 3A). Triple-staining with GFAP and DAPI depicted STAT3 immunofluorescence accumulated in the nuclear region of GFAP-positive astrocytes (Fig. 3B). Given the translocation of active STAT3 to the nucleus (Reich and Liu, 2006), these results suggested astrocytic activation of STAT3 in the compressed SDH. As STAT3 has also been reported to be activated in microglia (Dominguez et al., 2008), we examine STAT3 activation at a later timepoint after compression. However, there was no co-localization of STAT3 and OX-42 (a marker of microglia) immunofluorescence on day 14 after compression (Sup. 5).

To determine whether astrocytic STAT3 activation was required for remote mechanical pain after spinal cord compression, a dominant negative form of STAT3 (dnSTAT3, a mutant of STAT3 carrying phenylalanine substitution at Tyr705, which interferes with STAT3 activation) (Bonni et al., 1997) was specifically expressed in astrocytes located at the compressed SDH using an established method for minimally invasive microinjection of rAAV vector into the SDH (Kohro et al., 2015). An AAV2/5 vector (a serotype with preferential tropism for astrocytes) (Ortinski et al., 2010) designed to express either dnSTAT3 or GFP under the control of the astrocytic promoter gfaABC$_1$D (Haustein et al., 2014; Lee et al., 2008; Shigetomi et al., 2013; Tong et al., 2014; Xie et al., 2010) was microinjected unilaterally into the L1 segment of the SDH (Fig. 4A). In spinal cord-compressed mice administered AAV–gfaABC$_1$D-GFP, strong GFP fluorescence was still evident on the side of the compression but not on the contralateral side 28 days after AAV injection (Fig. 4B). While strong GFP fluorescence was observed in the injected area, GFP expression in the superficial layer was confirmed by immunohistochemistry using a GFP antibody (Fig. 4B). GFP fluorescence was not observed in the Th13 and L2 segments (Fig. 4C). GFP$^+$ cells were double-stained with GFAP and SOX9

(Fig. 4D), both of which are markers of astrocytes, and 99% of total GFP$^+$ cells (72/73 cells) exhibited SOX9 immunofluorescence. No colocalization of GFP with cells positive for IBA1 (a microglial marker), NeuN (a neuronal marker), or APC (an oligodendrocyte marker) was observed (Fig. 4D). These results strongly suggest that intra-SDH microinjection of AAV-gfaABC$_1$D vector facilitated selective gene expression in astrocytes at the site of the compressed SDH. This method was used to induce dnSTAT3 expression in astrocytes at the site of the compressed SDH via microinjection of AAV-gfaABC$_1$D-dnSTAT3. Consistent with previously reported data derived from other models (Kohro et al., 2015), the spinal cord compression-induced increase in GFAP immunoreactivity was significantly suppressed in mice injected with AAV-gfaABC$_1$D-dnSTAT3 compared with mice injected with AAV-gfaABC$_1$D-GFP (Fig. 4E, F), indicating that dnSTAT3 expression suppressed astrocytic activation caused by SDH compression. Furthermore, dnSTAT3 expression prevented the development of remote spinal cord compression-induced mechanical pain in both hindpaws compared with GFP (Fig. 4G, H). In contrast, prevention of mechanical pain in hindpaws was not observed in spinal cord-compressed mice in which dnSTAT3 had been expressed in SDH astrocytes at the site of the L4 segment (Sup. 6). These results suggested that astrocytes at the site of spinal cord compression were involved in the induction of remote mechanical pain observed in the hindpaws.

Furthermore, to examine whether astrocytic STAT3 activation in the L1 SDH produces remote mechanical pain, AAV-gfaABC$_1$D vector containing a constitutively active form of STAT3 (caSTAT3) or GFP was microinjected unilaterally into the L1 SDH of naive mice. Similar to mice expressing GFP, the withdrawal threshold of the hindpaws in mice with caSTAT3 expression was not changed (Fig. 4I), suggesting that astrocytic STAT3 activation in the L1 segment alone is not sufficient to produce remote mechanical pain.
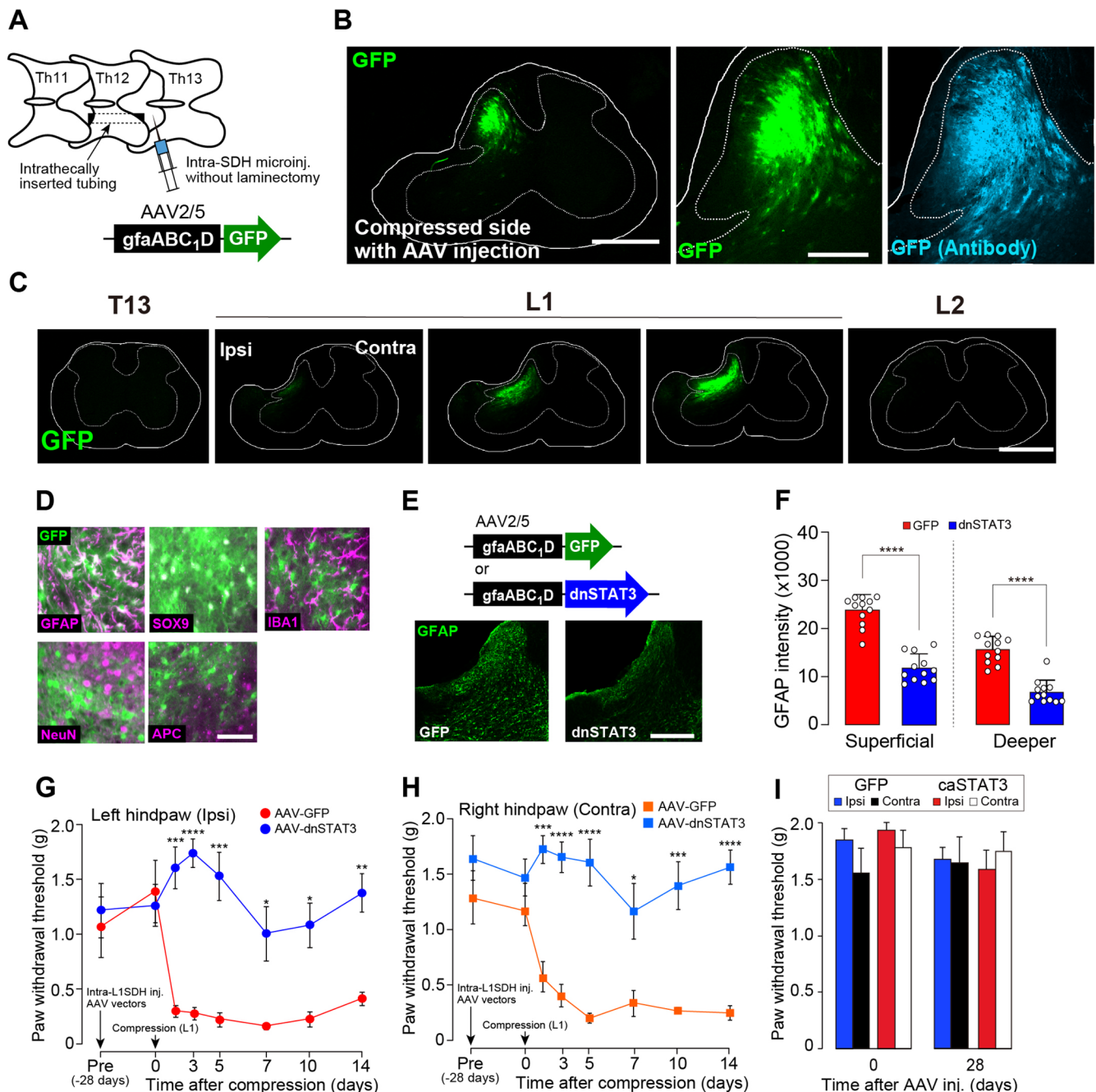
Fig. 4. Astrocytic dnSTAT3 expression in the compressed SDH prevented bilateral remote mechanical hindpaw pain. (A) Schematic illustration of micro-injection into the compressed SDH (L1 segment) of the AAV vector designed to express GFP under the control of an astrocyte-selective promoter (gfaABC$_1$D). (B) Representative images of GFP fluorescence and immunofluorescence (detected by GFP antibody) in the L1 SDH of mice with AAV-gfaABC$_1$D-GFP on day 3 after compression. (C) Images of GFP fluorescence in the spinal cord at the T13, L1 and L2 regions of mice with AAV-gfaABC$_1$D-GFP on day 3 after compression. (D) Immunohistochemical identification of GFP-expressing cells using cell type-specific markers (green, GFP; magenta, GFAP, SOX9, IBA1, NeuN, and APC) in the compressed L1 SDH of mice with AAV-gfaABC$_1$D-GFP. (E) Representative images of GFAP immunofluorescence in the L1 SDH of mice injected with AAV-gfaABC$_1$D-GFP or -dnSTAT3 14 days after the compression. (F) Quantitative analyses of GFAP immunofluorescence intensity in the L1 SDH of mice injected with AAV-gfaABC$_1$D-GFP or -dnSTAT3 14 days after compression. ****$P < 0.0001$, Mann-Whitney U test. (G, H) PWT in the left (ipsilateral; G) and right (contralateral; H) hindpaws of mice injected with AAV-gfaABC$_1$D-GFP ($n = 10$) or -dnSTAT3 ($n = 6$) at pre-AAV injection (day -28), before (day 0) and after spinal cord compression. *$P < 0.05$, **$P < 0.01$, ***$P < 0.001$ and ****$P < 0.0001$ versus the value of AAV-gfaABC$_1$D-GFP-injected group, two-way ANOVA with post hoc Bonferroni test. (I) PWT of AAV-gfaABC$_1$D-GFP ($n = 6$) or -caSTAT3 ($n = 7$) injected mice before (day 0) and after AAV injection. Two-way ANOVA with post hoc Bonferroni test. Data show mean $\pm$ SEM. Scale bars, 500 μm (B, C), 200 μm (B (middle), E), 50 μm (D). (For interpretation of the references to colour in this figure legend, the reader is referred to the web version of this article.)

3.3. Intrathecal IL-6-neutralizing antibody reversed spinal cord compression-induced remote pain

Because reactive astrocytes secrete various factors that modulate

pain signaling in the SDH, particularly proinflammatory cytokines, it was surmised that the spinal cord compression-induced remote pain evident in the present study may involve proinflammatory cytokines secreted by astrocytes at the compressed site. Factors investigated
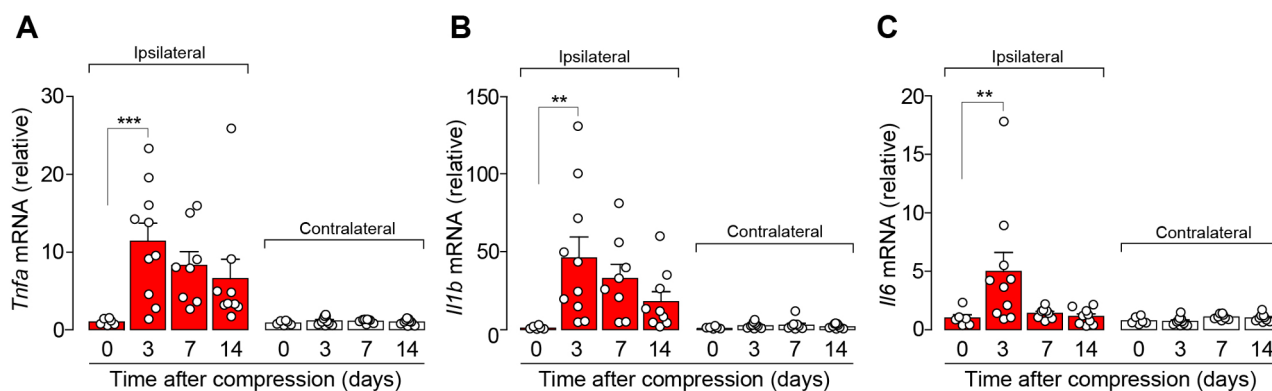
Fig. 5. Spinal cord compression upregulated the expression of proinflammatory cytokines in the L1 segment. Real-time PCR analysis of *Tnfa*, *Il1b* and *Il6* mRNAs at the L1 segment of mice before (day 0) and after spinal cord compression. Values represent the relative ratio of mRNA (normalized to the average of *Gapdh* and *Actb* mRNA levels) to the value of day 0 (day 0 (naïve), n = 6; day 3, n = 10; day 7, n = 8; day 14, n = 9). **P < 0.01 and ***P < 0.001, one-way ANOVA with Tukey's multiple comparison test. Data show mean ± SEM.
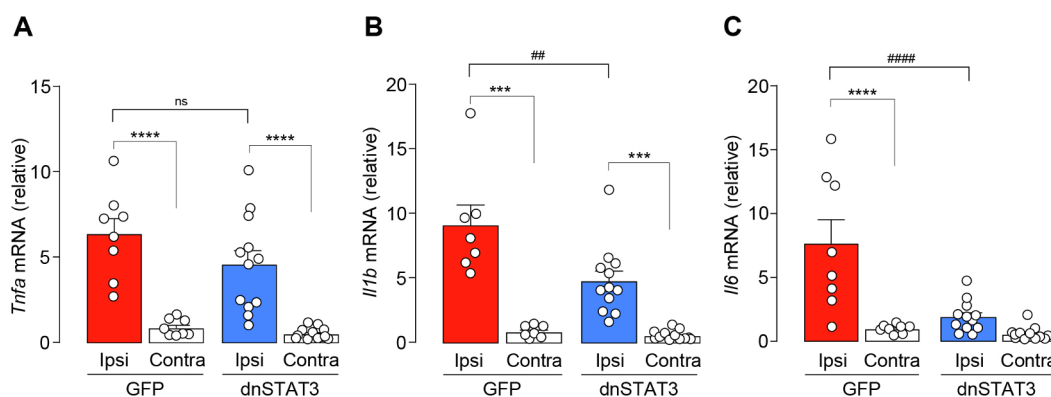

Fig. 6. Astrocytic expression of dnSTAT3 suppressed compression-induced upregulation of IL-6 and IL-1β. Real-time PCR analysis of *Tnfa*, *Il1b* and *Il6* mRNAs in L1 spinal segment of mice injected with AAV-gfaABC₁D-GFP (n = 7–8) or -dnSTAT3 (n = 12) on day 3 after spinal cord compression. Values represent the relative ratio of mRNA (normalized to *Gapdh* and *Actb* mRNA) to the contralateral side of AAV-gfaABC₁D-GFP-injected group. Ipsi, ipsilateral; Contra, contralateral. ***P < 0.001, ****P < 0.0001, ##P < 0.01 and ####P < 0.0001, one-way ANOVA with Tukey's multiple comparison test. Data show mean ± SEM.

included TNFα, IL-1β, and IL-6, and mRNA levels of all three of these cytokines were increased in spinal cords 3 days after compression (Fig. 5A–C). Upregulation of *Il6* and *Il1b* gene expression was significantly reduced by astrocyte-specific expression of dnSTAT3 at the site of SDH compression (Fig. 6A–C), suggesting involvement of STAT3 in the expression of these genes.

Whether proinflammatory cytokines contribute to remote pain was investigated in the present study. Because IL-6 upregulation was markedly suppressed by dnSTAT3 (Fig. 6C), the effects of IL-6-neutralizing antibody were assessed. A single intrathecal injection of IL-6-neutralizing antibody at day 3 after spinal cord compression reversed the remote mechanical pain of the left (ipsilateral) hindpaw. This suppressive effect lasted for several hours, and mechanical pain had returned to pre-injection levels 1 day thereafter (Fig. 7A, B). A similar reversal of mechanical pain was also observed in the right (contralateral) hindpaw. The effect of IL-6 antibody seemed slightly smaller in the ipsilateral hindpaw than the contralateral hindpaw, but there was no significant difference between the two groups. In contrast to the reversal effect of IL–6–neutralizing antibody, mechanical pain was not suppressed by a single intrathecal injection of IL–1β–neutralizing antibody on day 3 after compression (Fig. 7C, D), at a dose that has been reported to suppress mechanical hypersensitivity by peripheral nerve injury (Kawasaki et al., 2008a). These results imply that IL-6 upregulation via astrocytic STAT3 signaling at the site of the compressed SDH plays a pivotal role in the induction of bilateral remote mechanical pain in the hindpaws of mice in this experimental model.

4. Discussion

In the current study, spinal cord compression-induced remote pain was investigated in a mouse model in which the spinal cord was compressed via the physical insertion of flexible tubing with a small external diameter. Compared with previous methods involving the use of polyether sheeting to compress the spinal cord, the method used in the present study results in constant compression of the spinal cord, and facilitates much easier and more rapid induction of targeted compression without substantial unintended tissue damage. The tubing insertion method utilized in the present study does not require laminectomy, which typically results in an inflammatory response and extensive tissue damage. In stark contrast with other models of spinal cord injury, it also does not entail a cavity in the compressed spinal cord. Notably, the mechanical pain induced in the model described herein was reliably reproducible. Thus, the model may be useful for investigating the effects of spinal cord compression alone on pain responses, in the absence of additional secondary effects that arise as consequences of massive tissue injury.

Using the above-described model, we demonstrated for the first time that spinal cord compression-induced remote mechanical pain is associated with reactive astrocytes in the compressed region. Activation of astrocytes in the compressed SDH has been reported previously (Moon et al., 2014), but its functional consequences in chronic pain have not been elucidated. In the current study, suppressing reactive astrocytes by inhibiting STAT3 signaling in the compressed SDH by dnSTAT3 prevented remote mechanical pain responses. dnSTAT3 inhibits
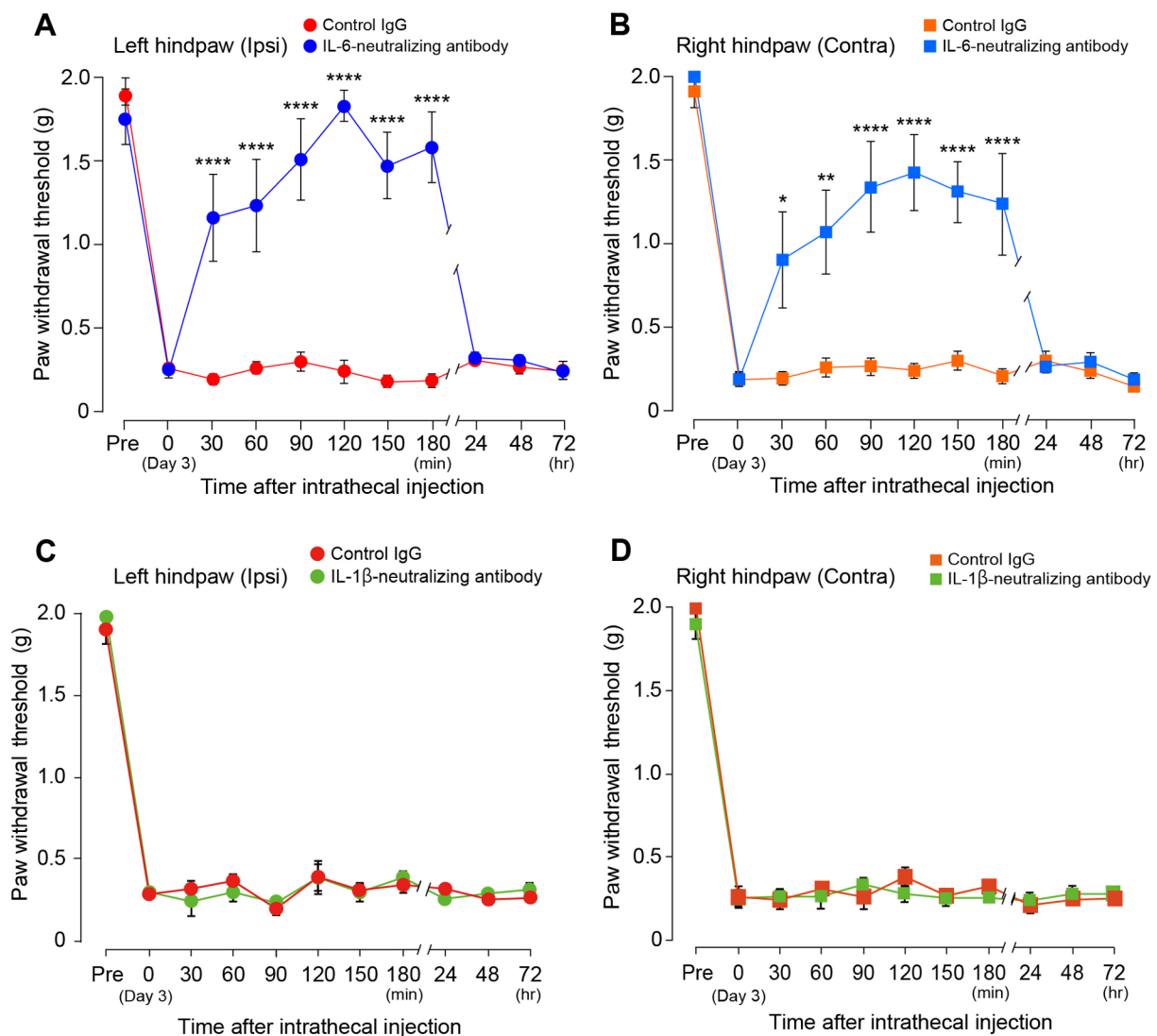
Fig. 7. Intrathecal injection of IL-6-neutralizing antibody reversed remote mechanical pain induced by spinal cord compression. PWT measured before (Pre) and 3 days after spinal cord compression (0), and after the intrathecal injection of IL-6-neutralizing antibody ($n = 6$) or an IgG control ($n = 5$) (A, B) and IL-1β-neutralizing antibody or an IgG control ($n = 5$) (C, D). *P < 0.05, **P < 0.01, and ****P < 0.0001 versus the value of each timepoint of IgG-treated group, two-way ANOVA with post hoc Bonferroni test. Data show mean ± SEM.

phosphorylation of Tyr705 STAT3 and interferes with its activation (Bonni et al., 1997). As STAT3 plays as a key inducer of astrocyte reactivity through various cellular and molecular changes, for example hypertrophic morphology and gene expression such as GFAP and other proinflammatory cytokines including IL-6 (Ceyzeriat et al., 2016), dnSTAT3 can inhibit such reactive processes. In fact, GFAP immunofluorescence expression and upregulation of IL-1β and IL-6 in the compressed region of the spinal cord were suppressed by astrocyte-selective expression of dnSTAT3. Furthermore, remote pain was reversed via intrathecal administration of an IL–6–neutralizing antibody. Whether IL-6 is expressed by reactive astrocytes in humans remains to be determined, but previous studies suggest that they release IL-6 in diverse rodent models of CNS diseases (Zhou et al., 2016), and that STAT3 directly regulates IL-6 gene expression in astrocytes (Huang et al., 2010; Kandalam and Clark, 2010; Wang et al., 2012); presumably via direct binding to its promoter region (Kang et al., 2012; Yoon et al., 2010; Yoon et al., 2012). Collectively these findings suggest that spinal cord compression-induced remote mechanical pain may involve IL-6 derived from reactive astrocytes in the compressed region.

The mechanism underlying how astrocytic IL-6 in the compressed L1 spinal cord contributes to remote mechanical pain of the hindpaws remains unclear, but two hypotheses could be considered. The first one is that astrocyte-derived IL-6 in the L1 compressed spinal cord may diffuse to neighboring segments via the cerebrospinal fluid, which in turn enhances spinal pain transmission and induces mechanical hypersensitivity of the hindpaws. This hypothesis was supported in part by no alteration in IL-6 mRNA levels in the L4 SDH after L1 spinal compression (Sup. 7) and by no effect of astrocytic dnSTAT3 expression in the L4 segment on remote mechanical pain (Sup. 6). Furthermore, previous studies have reported that intrathecal IL-6 administration in normal animals induced mechanical pain (DeLeo et al., 1996; Wen et al., 2011). Electrophysiological studies have also indicated that IL-6 can enhance excitatory synaptic responses in SDH neurons (Ikeda et al., 2007; Kawasaki et al., 2008b). However, IL-6 protein in isolated L1 spinal cord tissues was not detected in ELISA experiments (data not shown). Thus, as the second hypothesis, it is conceivable that astrocytic IL-6 may act locally in the L1 spinal cord rather than remotely affecting the L4 segment. Spinal IL-6 has been implicated in producing other inflammatory factors (presumably via astrocytes themselves and microglia) (Schoeniger-Skinner et al., 2007; Serizawa et al., 2018) that can enhance spinal pain transmission (Grace et al., 2014; Inoue and Tsuda, 2018; Ji et al., 2014). IL-6-stimulated astrocytes have been

shown to induce the chemokine CCL7 (Imai et al., 2013), an agonist for the chemokine receptor CCR2 that is implicated in recruiting monocytes/macrophages (Chu et al., 2014). Indeed, monocytes/macrophages and CD4^{+} T-cells infiltrated into the compressed L1 spinal cord. These infiltrating immune cells are also implicated in pain hypersensitivity via a release of inflammatory factors (Grace et al., 2014; Ji et al., 2014). Thus, it is speculated that neuroinflammation elicited by interactions between astrocytes and other cell types (microglia and infiltrated immune cells), via IL-6 and other factors, in the compressed L1 spinal segment may spread to surrounding regions including the L4 segment, inducing remote mechanical pain of the hindpaws by altering pain processing. The detailed mechanism underlying this interaction and its role in remote pain remains unclear, but in the future it would be important to clarify this point by focusing on the role of these cell types.

Although in the current study the levels of *Aif1* and *Itgam* mRNA at the L4 segment were not altered at any of the timepoints investigated after compression at L1 except day 3 (Sup. 8), involvement of microglia in the L4 SDH in remote mechanical pain cannot be excluded. It is also notable that as well as IL-6, spinal cord compression was associated with upregulation of other proinflammatory cytokines including TNFα and IL-1β. Both of these cytokines have been implicated in chronic pain (Ikeda et al., 2007; Ji et al., 2014; Leung and Cahill, 2010; Lu et al., 2014; Watkins et al., 2001), but intrathecal injection of IL–1β–neutralizing antibody on day 3 after compression had no effect on mechanical pain, suggesting that spinal IL–1β is not responsible for compression-induced remote pain, at least at that timepoint.

A surprising finding in the present study was that remote mechanical pain spontaneously resolved approximately 5 weeks after the compression, even though the spinal cord remained compressed. The reason for this is unclear but GFAP levels also returned to basal level, suggesting that reactive astrocytes may have subsided in the late phase, contributing to recovery from pain.

Patients with spinal cord compression frequently complain of numbness as well as chronic pain (Barnett et al., 1987). It has also been reported that in a preclinical mouse model numbness can be evaluated via licking and biting behaviors (So et al., 2016). No changes in licking or biting behaviors were observed in the present study after the infliction of spinal cord compression. To the best of our knowledge, there is no rodent model of spinal cord compression that elicits licking and biting behaviors. The development of a preclinical model of spinal cord compression-induced numbness may prove informative in the future.

In summary, in the current study a mouse model of constant compression of the spinal cord without direct massive injury resulted in reproducible induction of remote mechanical pain behavior, and STAT3-dependent reactive astrocytes and IL-6 in the compressed spinal cord evidently contributed to remote mechanical pain in the lower extremity. These results suggest a mechanism underlying spinal cord compression-induced remote pain, and may also provide a target for treating chronic pain in spinal disorders associated with spinal cord compression such as spinal canal stenosis and cervical spondylotic myelopathy.

Author contributions

T.O. designed and performed most experiments, analyzed the data and wrote the manuscript. Y.K., H.T.-S. advised on some experiments using AAV vector. K.K. performed flow cytometry experiments. Y.N. provided critical comments on this study. M.T. conceived this project, designed the experiments, supervised the overall project, and wrote the manuscript.

Declaration of Competing Interest

The authors declare no competing financial interests.

Appendix A. Supplementary data

Supplementary data to this article can be found online at https://doi.org/10.1016/j.bbi.2020.07.025.

References

Ayuso, E., Mingozzi, F., Montane, J., Leon, X., Anguela, X.M., Haurigot, V., Edmonson, S.A., Africa, L., Zhou, S., High, K.A., Bosch, F., Wright, J.F., 2010. High AAV vector purity results in serotype- and tissue-independent enhancement of transduction efficiency. Gene Ther. 17 (4), 503–510.
Barnett, G.H., Hardy Jr., R.W., Little, J.R., Bay, J.W., Sypert, G.W., 1987. Thoracic spinal canal stenosis. J. Neurosurg. 66 (3), 338–344.
Basso, D.M., Fisher, L.C., Anderson, A.J., Jakeman, L.B., McTigue, D.M., Popovich, P.G., 2006. Basso Mouse Scale for locomotion detects differences in recovery after spinal cord injury in five common mouse strains. J. Neurotrauma 23 (5), 635–659.
Bonni, A., Sun, Y., Nadal-Vicens, M., Bhatt, A., Frank, D.A., Rozovsky, I., Stahl, N., Yancopoulos, G.D., Greenberg, M.E., 1997. Regulation of gliogenesis in the central nervous system by the JAK-STAT signaling pathway. Science 278 (5337), 477–483.
Ceyzeriat, K., Abjean, L., Carrillo-de Sauvage, M.A., Ben Haim, L., Escartin, C., 2016. The complex STATes of astrocyte reactivity: how are they controlled by the JAK-STAT3 pathway? Neuroscience 330, 205–218.
Chan, C.K., Lee, H.Y., Choi, W.C., Cho, J.Y., Lee, S.H., 2011. Cervical cord compression presenting with sciatica-like leg pain. Eur. Spine J. 20 (Suppl 2), S217–S221.
Chaplan, S.R., Bach, F.W., Pogrel, J.W., Chung, J.M., Yaksh, T.L., 1994. Quantitative assessment of tactile allodynia in the rat paw. J. Neurosci. Methods 53 (1), 55–63.
Chu, H.X., Arumugam, T.V., Gelderblom, M., Magnus, T., Drummond, G.R., Sobey, C.G., 2014. Role of CCR2 in inflammatory conditions of the central nervous system. J. Cereb. Blood Flow Metab. 34 (9), 1425–1429.
DeLeo, J.A., Colburn, R.W., Nichols, M., Malhotra, A., 1996. Interleukin-6-mediated hyperalgesia/allodynia and increased spinal IL-6 expression in a rat mononeuropathy model. J. Interferon Cytokine Res. 16 (9), 695–700.
Dominguez, E., Rivat, C., Pommier, B., Mauborgne, A., Pohl, M., 2008. JAK/STAT3 pathway is activated in spinal cord microglia after peripheral nerve injury and contributes to neuropathic pain development in rat. J. Neurochem. 107 (1), 50–60.
Grace, P.M., Hutchinson, M.R., Maier, S.F., Watkins, L.R., 2014. Pathological pain and the neuroimmune interface. Nat. Rev. Immunol. 14 (4), 217–231.
Haustein, M.D., Kracun, S., Lu, X.H., Shih, T., Jackson-Weaver, O., Tong, X.P., Xu, J., Yang, X.W., O'Dell, T.J., Marvin, J.S., Ellisman, M.H., Bushong, E.A., Looger, L.L., Khakh, B.S., 2014. Conditions and constraints for astrocyte calcium signaling in the hippocampal mossy fiber pathway. Neuron 82 (2), 413–429.
Herrmann, J.E., Imura, T., Song, B., Qi, J., Ao, Y., Nguyen, T.K., Korsak, R.A., Takeda, K., Akira, S., Sofroniew, M.V., 2008. STAT3 is a critical regulator of astrogliosis and scar formation after spinal cord injury. J. Neurosci. 28 (28), 7231–7243.
Huang, W.L., Yeh, H.H., Lin, C.C., Lai, W.W., Chang, J.Y., Chang, W.T., Su, W.C., 2010. Signal transducer and activator of transcription 3 activation up-regulates interleukin-6 autocrine production: a biochemical and genetic study of established cancer cell lines and clinical isolated human cancer cells. Mol Cancer 9, 309.
Hylden, J.L., Wilcox, G.L., 1980. Intrathecal morphine in mice: a new technique. Eur. J. Pharmacol. 67 (2–3), 313–316.
Ikeda, H., Tsuda, M., Inoue, K., Murase, K., 2007. Long-term potentiation of neuronal excitation by neuron-glia interactions in the rat spinal dorsal horn. Eur. J. Neurosci. 25 (5), 1297–1306.
Imai, S., Ikegami, D., Yamashita, A., Shimizu, T., Narita, M., Niikura, K., Furuya, M., Kobayashi, Y., Miyashita, K., Okutsu, D., Kato, A., Nakamura, A., Araki, A., Omi, K., Nakamura, M., James Okano, H., Okano, H., Ando, T., Takeshima, H., Ushijima, T., Kuzumaki, N., Suzuki, T., Narita, M., 2013. Epigenetic transcriptional activation of monocyte chemotactic protein 3 contributes to long-lasting neuropathic pain. Brain 136 (Pt 3), 828–843.
Inoue, K., Tsuda, M., 2018. Microglia in neuropathic pain: cellular and molecular mechanisms and therapeutic potential. Nat. Rev. Neurosci. 19 (3), 138–152.
Ito, T., Homma, T., Uchiyama, S., 1999. Sciatica caused by cervical and thoracic spinal cord compression. Spine 24 (12), 1265–1267.
Ji, R.R., Donnelly, C.R., Nedergaard, M., 2019. Astrocytes in chronic pain and itch. Nat. Rev. Neurosci. 20 (11), 667–685.
Ji, R.R., Xu, Z.Z., Gao, Y.J., 2014. Emerging targets in neuroinflammation-driven chronic pain. Nat. Rev. Drug Discov. 13 (7), 533–548.
Kandalam, U., Clark, M.A., 2010. Angiotensin II activates JAK2/STAT3 pathway and induces interleukin-6 production in cultured rat brainstem astrocytes. Regul. Pept. 159 (1–3), 110–116.

Kang, J.W., Park, Y.S., Lee, D.H., Kim, J.H., Kim, M.S., Bak, Y., Hong, J., Yoon, D.Y., 2012. Intracellular interaction of interleukin (IL)-32alpha with protein kinase Cepsilon (PKCepsilon) and STAT3 protein augments IL-6 production in THP-1 promonocytic cells. J. Biol. Chem. 287 (42), 35556–35564.

Kawasaki, Y., Xu, Z.Z., Wang, X., Park, J.Y., Zhuang, Z.Y., Tan, P.H., Gao, Y.J., Roy, K., Corfas, G., Lo, E.H., Ji, R.R., 2008a. Distinct roles of matrix metalloproteases in the early- and late-phase development of neuropathic pain. Nat. Med. 14 (3), 331–336.

Kawasaki, Y., Zhang, L., Cheng, J.K., Ji, R.R., 2008b. Cytokine mechanisms of central sensitization: distinct and overlapping role of interleukin-1beta, interleukin-6, and tumor necrosis factor-alpha in regulating synaptic and neuronal activity in the superficial spinal cord. J. Neurosci. 28 (20), 5189–5194.

Koga, K., Kanehisa, K., Kohro, Y., Shiratori-Hayashi, M., Tozaki-Saitoh, H., Inoue, K., Furue, H., Tsuda, M., 2017. Chemogenetic silencing of GABAergic dorsal horn interneurons induces morphine-resistant spontaneous nocifensive behaviours. Sci. Rep. 7 (1), 4739.

Kohro, Y., Sakaguchi, E., Tashima, R., Tozaki-Saitoh, H., Okano, H., Inoue, K., Tsuda, M., 2015. A new minimally-invasive method for microinjection into the mouse spinal dorsal horn. Sci. Rep. 5.

Lee, Y., Messing, A., Su, M., Brenner, M., 2008. GFAP promoter elements required for region-specific and astrocyte-specific expression. Glia 56 (5), 481–493.

Leung, L., Cahill, C.M., 2010. TNF-alpha and neuropathic pain–a review. J Neuroinflammation 7, 27.

Lock, M., Alvira, M., Vandenberghe, L.H., Samanta, A., Toelen, J., Debyser, Z., Wilson, J.M., 2010. Rapid, simple, and versatile manufacturing of recombinant adeno-associated viral vectors at scale. Hum. Gene Ther. 21 (10), 1259–1271.

Lu, Y., Jiang, B.C., Cao, D.L., Zhang, Z.J., Zhang, X., Ji, R.R., Gao, Y.J., 2014. TRAF6 upregulation in spinal astrocytes maintains neuropathic pain by integrating TNF-alpha and IL-1beta signaling. Pain 155 (12), 2618–2629.

Moon, E.S., Karadimas, S.K., Yu, W.R., Austin, J.W., Fehlings, M.G., 2014. Riluzole attenuates neuropathic pain and enhances functional recovery in a rodent model of cervical spondylotic myelopathy. Neurobiol. Dis. 62, 394–406.

Morioka, N., Fujii, S., Kondo, S., Zhang, F.F., Miyauchi, K., Nakamura, Y., Hisaoka-Nakashima, K., Nakata, Y., 2018. Downregulation of spinal astrocytic connexin43 leads to upregulation of interleukin-6 and cyclooxygenase-2 and mechanical hypersensitivity in mice. Glia 66 (2), 428–444.

Okada, S., Nakamura, M., Katoh, H., Miyao, T., Shimazaki, T., Ishii, K., Yamane, J., Yoshimura, A., Iwamoto, Y., Toyama, Y., Okano, H., 2006. Conditional ablation of Stat3 or Socs3 discloses a dual role for reactive astrocytes after spinal cord injury. Nat. Med. 12 (7), 829–834.

Ortinski, P.I., Dong, J.H., Mungenast, A., Yue, C.Y., Takano, H., Watson, D.J., Haydon, P.G., Coulter, D.A., 2010. Selective induction of astrocytic gliosis generates deficits in neuronal inhibition. Nat. Neurosci. 13 (5), 584–U93.

Reich, N.C., Liu, L., 2006. Tracking STAT nuclear traffic. Nat. Rev. Immunol. 6 (8), 602–612.

Schoeniger-Skinner, D.K., Ledeboer, A., Frank, M.G., Milligan, E.D., Poole, S., Martin, D., Maier, S.F., Watkins, L.R., 2007. Interleukin-6 mediates low-threshold mechanical allodynia induced by intrathecal HIV-1 envelope glycoprotein gp120. Brain Behav.

Immun. 21 (5), 660–667.

Serizawa, K., Tomizawa-Shinohara, H., Magi, M., Yogo, K., Matsumoto, Y., 2018. Anti-IL-6 receptor antibody improves pain symptoms in mice with experimental autoimmune encephalomyelitis. J. Neuroimmunol. 319, 71–79.

Shigetomi, E., Bushong, E.A., Haustein, M.D., Tong, X.P., Jackson-Weaver, O., Kracun, S., Xu, J., Sofroniew, M.V., Ellisman, M.H., Khakh, B.S., 2013. Imaging calcium microdomains within entire astrocyte territories and endfeet with GCaMPs expressed using adeno-associated viruses. J. Gen. Physiol. 141 (5), 633–647.

So, K., Tei, Y., Zhao, M., Miyake, T., Hiyama, H., Shirakawa, H., Imai, S., Mori, Y., Nakagawa, T., Matsubara, K., Kaneko, S., 2016. Hypoxia-induced sensitisation of TRPA1 in painful dysesthesia evoked by transient hindlimb ischemia/reperfusion in mice. Sci. Rep. 6, 23261.

Tashima, R., Mikuriya, S., Tomiyama, D., Shiratori-Hayashi, M., Yamashita, T., Kohro, Y., Tozaki-Saitoh, H., Inoue, K., Tsuda, M., 2016. Bone marrow-derived cells in the population of spinal microglia after peripheral nerve injury. Sci. Rep. 6, 23701.

Tong, X.P., Ao, Y., Faas, G.C., Nwaobi, S.E., Xu, J., Haustein, M.D., Anderson, M.A., Mody, I., Olsen, M.L., Sofroniew, M.V., Khakh, B.S., 2014. Astrocyte Kir4.1 ion channel deficits contribute to neuronal dysfunction in Huntington's disease model mice. Nat. Neurosci. 17 (5), 694-+.

Tsuda, M., Kohro, Y., Yano, T., Tsujikawa, T., Kitano, J., Tozaki-Saitoh, H., Koyanagi, S., Ohdo, S., Ji, R.R., Salter, M.W., Inoue, K., 2011. JAK-STAT3 pathway regulates spinal astrocyte proliferation and neuropathic pain maintenance in rats. Brain 134 (Pt 4), 1127–1139.

Vandenberghe, L.H., Xiao, R., Lock, M., Lin, J., Korn, M., Wilson, J.M., 2010. Efficient serotype-dependent release of functional vector into the culture medium during adeno-associated virus manufacturing. Hum. Gene Ther. 21 (10), 1251–1257.

Wang, J., Li, G., Wang, Z., Zhang, X., Yao, L., Wang, F., Liu, S., Yin, J., Ling, E.A., Wang, L., Hao, A., 2012. High glucose-induced expression of inflammatory cytokines and reactive oxygen species in cultured astrocytes. Neuroscience 202, 58–68.

Watkins, L.R., Milligan, E.D., Maier, S.F., 2001. Glial activation: a driving force for pathological pain. Trends Neurosci. 24 (8), 450–455.

Wen, Y.R., Tan, P.H., Cheng, J.K., Liu, Y.C., Ji, R.R., 2011. Microglia: a promising target for treating neuropathic and postoperative pain, and morphine tolerance. J. Formos. Med. Assoc. 110 (8), 487–494.

Xie, Y., Wang, T., Sun, G.Y., Ding, S., 2010. Specific disruption of astrocytic Ca2+ signaling pathway in vivo by adeno-associated viral transduction. Neuroscience 170 (4), 992–1003.

Yoon, S., Woo, S.U., Kang, J.H., Kim, K., Kwon, M.H., Park, S., Shin, H.J., Gwak, H.S., Chwae, Y.J., 2010. STAT3 transcriptional factor activated by reactive oxygen species induces IL6 in starvation-induced autophagy of cancer cells. Autophagy 6 (8), 1125–1138.

Yoon, S., Woo, S.U., Kang, J.H., Kim, K., Shin, H.J., Gwak, H.S., Park, S., Chwae, Y.J., 2012. NF-kappaB and STAT3 cooperatively induce IL6 in starved cancer cells. Oncogene 31 (29), 3467–3481.

Zhou, Y.Q., Liu, Z., Liu, Z.H., Chen, S.P., Li, M., Shahveranov, A., Ye, D.W., Tian, Y.K., 2016. Interleukin-6: an emerging regulator of pathological pain. J Neuroinflammation 13 (1), 141.